Viral templates for gold nanoparticle synthesis†

Joseph M. Slocik,[a] Rajesh R. Naik,[b] Morley O. Stone[b] and David W. Wright*[a]

Received 25th August 2004, Accepted 10th November 2004
First published as an Advance Article on the web 21st December 2004
DOI: 10.1039/b413074j

Viruses present a confined environment and unique protein surface topology (*i.e.* polarity, residue charge, and surface relief) for nanoparticle synthesis and are amenable to molecular biology manipulations. Consequently, we have examined the cowpea chlorotic mottle viruses of unmodified SubE (yeast), (HRE)-SubE engineered with interior HRE peptide epitopes (AHHAHHAAD), and wild-type as viral templates for the potentiated reduction and symmetry directed synthesis of gold nanoparticles. In the first approach, the viral capsid actively potentiated the reduction of $AuCl_4^-$ by electron transfer from surface tyrosine residues resulting in a gold nanoparticle decorated viral surface. Viral reduction appeared to be selective for gold as a collection of metal precursor substrates of Ag^+, Pt^{4+}, Pd^{4+}, and an insoluble Au^I complex were not reduced to zero-valent nanoclusters by virus. Alternatively, the viral capsid provided a template for the symmetry directed synthesis of Au^0 nanoparticles from a non-reducible gold precursor.

Introduction

Nature exhibits a great deal of structural diversity in the biosynthetic control of inorganic materials. Exemplars include small phytochelatin peptides used to detoxify heavy metals and large ferritin storage proteins which internally mineralize iron oxide particles. Small peptides feature programmable metal binding domains, whereas proteins offer exquisite structural control through large architectural scaffolds. These templates provide exceptional model systems for the biomimetic synthesis of various nanoparticles. In particular, ferritin and ferritin analogues have been shown to control mineralization of atypical metal substrates within the protein cage yielding encapsulated nanoparticles that retain the dimensions of the protein cavity.[1–4] Recently, viruses have been exploited as a constrained template to direct nanoparticle synthesis. As templates, viruses offer confined cages, high symmetry, robust functional protein capsids, unique structural architectures, repeating motifs, and are amenable to molecular biology manipulations.[5,6]

Common examples of viral templates include the wild-type tobacco mosaic virus (TMV)[7–9] and cowpea chlorotic mottle virus (CCMV).[5,6,10] Mann *et al.* have shown selective mineralization with rod-like TMV particles by manipulating the pH and electrostatic nature of the viral components resulting in Au^0 mineralization along the external viral envelope surface or Ag^0 mineralization within the interior hollow channel.[8] Alternatively, Young *et al.* have designed a CCMV virion cage with an anionic interior surface that preferentially binds Fe^{II} and Fe^{III} ions by genetically replacing the nine basic residues at the N-terminus with glutamic acid groups.[1] This resulted in the spatially controlled oxidative hydrolysis of size constrained iron oxide nanoparticles. Thus, by changing the electrostatic environment of the cage from cationic in its native state (stabilizes anionic RNA core) to anionic through genetic mutations, the efficacy of engineered CCMV particles as nanoparticle templates was demonstrated. Moreover, we present a divergent approach to viral mediated nanoparticle synthesis that utilizes the unique surface chemistry and topology of the capsid with the judicious selection of metal precursor (Au^I *vs.* Au^{III}, Cl^- ligands *vs.* $P(CH_3)_3$). We have examined the metal precursors of $AuCl_4^-$ and $AuClP(CH_3)_3$ with the empty capsid of SubE expressed in yeast, an engineered virus with HRE peptides (previously reported to bind and stabilize Au^0, Ag^0, Pt^0, and Cu^0 nanoparticles)[11,12] within the cavity of (HRE)-SubE, and the wild-type virus, in the synthesis of gold nanoparticles. Accordingly, viral mediated synthesis proceeded *via* two pathways; (1) the viral potentiated reduction of $AuCl_4^-$ from surface tyrosine residues of the viral capsid and (2) the reduction of virus loaded with an inorganic gold(I) precursor ($AuClPCH_3)_3$) with borohydride.

Experimental

Virus templates

The CCMV SubE expression plasmid is previously described.[5] The first nine N-terminal amino acids of SubE were replaced with the HRE sequence (AHHAHHAAD) using mutagenic oligonucleotide primers. The HRE-SubE fusion was confirmed by DNA sequencing. The HRE-SubE fusion was expressed and purified from *Pichia pastoris* (Invitrogen, Carlsbad, CA). The HRE-SubE virus particles were purified as follows. The cells were resuspended in homogenization buffer (0.2 M sodium acetate pH 4.8, 10 mM ascorbic acid, 10 mM EDTA) and ruptured in a bead beater using glass bead for 5 min. The extract was then centrifuged at 13 000 rpm for 20 min. The supernatant was collected and spun at 25 000 rpm for 2 h to make the virus particles into a pellet. The virus particles were resuspended in buffer A (0.1 M sodium acetate

† Electronic supplementary information (ESI) available: UV–vis spectra, absorbance/fluorescence time plots, titration plots, pH profile and TEM micrographs/histograms. See http://www.rsc.org/suppdata/jm/b4/b413074j/

*David.wright@vanderbilt.edu

pH 4.8, 1 mM sodium azide, 1 mM EDTA) and then applied onto 39% caesium chloride (prepared in buffer A) and centrifuged at 38 000 rpm at 4 °C for 18 h. The virus band was collected and dialyzed into 10 mM sodium phosphate buffer pH 7.5 or double distilled water. The presence of HRE-SubE in the collected fraction was confirmed by immunoblotting using polyclonal antibodies produced against purified CCMV and TEM analysis.

Peptide synthesis

Peptides were synthesized by standard Fmoc protocols on an Advanced Chemtech model 90 automated peptide synthesizer double coupling every amino acid. Crude peptides were purified by reversed phase HPLC on a Waters Prep LC 4000 system equipped with a 2487 Dual Absorbance Detector on a Waters Delta Pak C_{18} (30 × 300 mm) column. Dissolved ~20 mg in 5.0 mL of water–0.1% TFA and injected at a flow rate of 40 mL min^{-1} with a gradient of 10% water–0.1% TFA and 90% acetonitrile–0.1% TFA over 20 min monitored at a λ of 210 nm. Peptide sequences were confirmed by MALDI-TOF mass spectrometry.

Gold reduction assay

20 μL of (HRE)-SubE virus (0.2 μg μL^{-1}), 2 μL of SubE (yeast) (2 mg mL^{-1}) or 2 μL of wild-type (2 mg mL^{-1}) was added with 750 μL of double deionized water in a septum-sealed 1.00 mL quartz cuvette. 1.00×10^{-7} mol of 5 mM $HAuCl_4$ stock solution was immediately added to the cuvette and monitored over 4 h with the kinetics software package supplied with Agilent 8453 photodiode array spectrophotometer. Samples were scanned at 30 s intervals for 4 h at a wavelength of 550 nm. Additionally, this reduction assay was performed with 5 mM stock solutions of $AgNO_3$, H_2PtCl_4, and K_2PdCl_6 according to the conditions above for $HAuCl_4$. The control HRE peptide, and tyrosine peptides (YHRE, Y_4HRE, and YYY) were examined by adding 1.01×10^{-7} mol of peptide with 1.00×10^{-7} mol of $HAuCl_4$ in 750 μL of water and kinetically monitored at 550 nm as described above.

In parallel, the fluoresence of tyrosine from virus particles was explored by adding 5 μL of (HRE)-SubE virus, SubE (yeast), or wild-type to 200 μL of water in a Starna 225 μL nominal volume quartz micro-cell with a 3 mm pathlength. To the micro-cell, 5 μL of 5 mM $HAuCl_4$ was added, sealed to keep anaerobic, and monitored kinetically on a Varian Cary Eclipse Fluorometer with a single cell holder and a kinetic software package over 4 h. Scan parameters consisted of an excitation slit of 10 nm, an emission slit of 5 nm, an average time of 1 s, and a photomultiplier tube voltage of 800 V. The sample was excited at two wavelengths of 270 nm and 295 nm, while emission was measured at 352 nm at both excitations simultaneously. Fluorescence of the YYY/$AuCl_4^-$ reaction was also performed according to the method described above.

Reductive synthesis of $AuClP(CH_3)_3$/virus precursor

20 μL of SubE (yeast), (HRE)-SubE, and wild-type was added to 750 μL of water and 2 mg of solid $AuClP(CH_3)_3$ anaerobically along with a micro stir bar in a 1.5 mL microfuge tube. The virus and Au^I precursor were stirred for 18 h. After stirring, the mixture was centrifuged for 30 min at 10 000 RPM and the supernatant was removed from the unreacted solid $AuClP(CH_3)_3$. 50 μL of 5 mM $NaBH_4$ was then added dropwise to precursor-virus complex and incubated for 4 h.

Virus modification of (HRE)-SubE

10 μL of (HRE)-SubE virus was added with 2 μL of (DEPC) diethylpyrocarbonate (16 mM) in 0.5 mL of 50 mM phosphate buffer pH 6.0 and incubated for 16 h. Modification of histidine was detected spectrophotometrically at 240 nm. Excess DEPC was removed from modified virus by Centricon filtration (NMWL 5000/Millipore) with water and repeated. The purified modified virus in water was examined as above with $AuClP(CH_3)_3$.

TEM characterization

Au^0 nanoparticle/virus structures were examined on a Phillips CM 20T transmission electron microscope operating at 200 kV. TEM samples were prepared by pipetting one drop of solution onto a 3 mm diameter copper grid covered with carbon type A film (Ted Pella, Inc.). Samples were additionally negatively stained with a 2% uranyl acetate solution by floating the grid on a drop of stain and removing after 30 s.

Results and discussion

Virus mediated reduction

Addition of $AuCl_4^-$ to SubE (yeast), (HRE)-SubE, and wild-type virus led to the rapid reduction to form Au^0 nanoparticles (either aerobically or anaerobically) as monitored by the appearance of a strong plasmon resonance peak at 550 nm (Fig. 1). Successive additions of $AuCl_4^-$ yielded a maximal amount of gold reduced per virus particle of 61 989 Au^0 atoms (see electronic supplementary information (ESI) for details†). Consequently, sequence analysis of CCMV reveals the presence of four tyrosine residues in close proximity to the

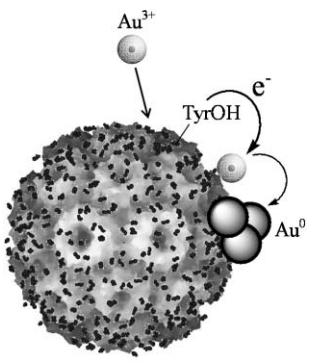

Fig. 1 Viral mediated reduction. $AuCl_4^-$ is added to virus, whereby a coupled deprotonation/electron transfer mechanism occurs with tyrosine at pH < 10 resulting in reduction of Au^{3+} to Au^0 nanoparticles. Virus picture is from http://chagall.scripps.edu/viper, while the viral tyrosines are from PDB 1CWP.[22]

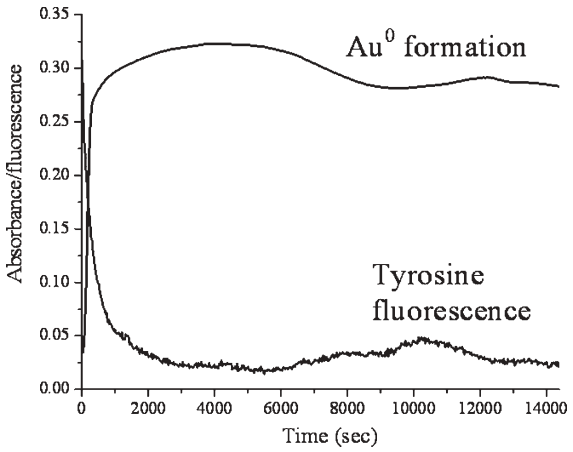

Fig. 2 Time plot of tyrosine fluorescence (ex. 270 nm/em. 352 nm) and plasmon absorption at 550 nm. Fluorescence intensities are normalized to absorbance.

C-terminus of each subunit that when assembled extends from the viral surface presenting multiple reduction sites.[22] When 180 of these subunits are assembled into the capsid, a total of 720 surface tyrosine residues representing 5.0×10^{14} electrons mol^{-1} are available for gold reduction. This provides a sufficient number of electrons for gold reduction and as a result limits Au^0 formation in the absence of external reductants. Other examples of gold reduction have been reported with hydroxyl-containing sugar-persubstituted poly-(amidoamine) dendrimers,[13] silk fibroin[14] rich in tyrosine residues, methanol,[15] and ethanol.[16]

We further substantiated the claim that tyrosine is indeed acting in gold reduction by following the decay of tyrosine's fluorescence as it is oxidized and quenched during the course of the reduction. The fluorescence was entirely quenched within 17 min of adding $AuCl_4^-$ and correlated with an increase in the plasmon absorbance band of Au^0 nanoparticles (Fig. 2). A parallel loss in fluorescence was also observed from excitation (295 nm) of a complimentary tryptophan component due to complete energy transfer from Tyr → Trp (good fluorescence donor–acceptor pair) that occurs at a separation distance of less than 15 Å.[17] Examination of the spatial relationship between tyrosine and tryptophan reveals a paired spacing of 3–15 Å within the virus.[22]

This intrinsic gold reduction activity of tyrosine (Table 1) was also explored with a control set of peptides: HRE (AHHAHHAAD), **Y**HRE (YAHHAHHAAD), $\mathbf{Y}_4$HRE (YAHHYAHHYAADY), and **YYY**. The peptides of HRE and **Y**HRE displayed a lack of nanoparticle formation due to the absence of an endogenous reductant, while the $\mathbf{Y}_4$HRE peptide exhibited minor gold reduction. As some Au^{3+} is slowly reduced by the peptide most of the gold binds at the histidine sites, preventing immediate reduction. This suggests that the ratio of tyrosine to histidine residues is critical for reduction to occur and requires at least a 2 : 1 ratio as in the virus system. In contrast, the tyrosine tripeptide successfully mediated the formation of Au^0 nanoclusters when reacted at a 1 : 1 molar ratio (ESI†).

The viral selectivity for gold was also explored with a collection of metal precursors of Ag^+, $PdCl_6^{2-}$, $PtCl_6^{2-}$, and an insoluble Au^I complex of $AuClP(CH_3)_3$ as potential substrates (ESI†). None of the precursors were reduced by (HRE)-SubE or wild-type/SubE (yeast) comparable to that of Au^{III}. As each metal ion inherently bears a different standard reduction potential for reduction from M^{n+} to M^0, the reductions of Ag^+ and $PtCl_6^-$ are not electrochemically favored when evaluated with the pH dependent formal reduction potential of tyrosine (0.894 V at a pH of 7.5).[23,24] $PdCl_6^{2-}$, however, has a reduction potential almost equivalent in magnitude to $AuCl_4^-$ and should be effectively reduced by the virus. The lack of reduction of $PdCl_6^{2-}$ by virus is most likely due to the extra electron required to reduce Pd^{IV} in contrast to the three electron reduction of Au^{III}. In total, the lack of activity amongst the set of HRE modified and unmodified viruses suggest similar redox properties and selectivity for gold.

To further explain the redox properties and mechanism of virus mediated gold reduction, the reduction of gold was examined over the buffered pH range of 4.0–9.6. The pH profile of gold reduction by (HRE)-SubE demonstrated minimal activity over the pH region of 4.0–9.0 (ESI†). Although at higher pH and near the pK_a of tyrosine (10.0),[24] the amount of gold nanoparticles produced by the virus was substantial, but at the cost of a rapid reduction rate. This is consistent with a reduction mechanism proposed by Zhou *et al.* with silk fibroin, whereby gold reduction occurs *via* a phenoxide anion of tyrosine at a pH of 9–10 due to the increased electron density for the π–π^* transition contributing to electron transfer from Tyr to gold.[14] Consequently, the decreased reduction rate by both systems is a direct result of the formation of insoluble $Au(OH)_3$ at high pH, and represents the rate limiting step to the speciation of the soluble complex ion of $Au(OH)_4^-$. Below the pK_a of tyrosine (4.0–9.0),

Table 1 Gold reduction mediated by virus/peptides

Template	Sequence	Reduction activity[a]	TEM size[b] Au^0/nm	TEM size[c] with reductant/nm
SubE (yeast)	CCMV Virus	+++	9.2 ± 3.9	3.2 ± 0.9
(HRE)-SubE	CCMV Virus	+++	8.3 ± 2.6	6.2 ± 2.0
Wild-type	CCMV Virus w/RNA	+++	23.8 ± 14.5	4.3 ± 1.3
HRE	AHHAHHAAD	—	NA	7.8 ± 1.7
YHRE	**Y**AHHAHHAAD	—	NA	2.7 ± 0.7
Y_4HRE	**Y**AHH**Y**AHH**Y**AAD**Y**	+	5.3 ± 2.1	NA
YYY	**YYY**	++	5.2 ± 1.9	4.0 ± 2.1

[a] Absorbance monitored at 550 nm with addition of $AuCl_4^-$ over 4 h; (+++) indicates extensive gold reduction, (++) moderate gold reduction, (+) minor reduction, (—) no reduction. [b] TEM sizes are from viral/peptide mediated reduction of $AuCl_4^-$ with no reductant added. NA indicates not applicable. [c] Borohydride reduction of $AuClP(CH_3)_3$ bound virus/peptide precursors.

where the surface tyrosine residues are protonated, gold reduction proceeds according to a coupled electron transfer/deprotonation mechanism. Such is the reported case for the redox process in photosystem II, whereby electron transfer from Tyr_z to $P680^+$ follows such a mechanism.[23] Due to the different pH regimes, both mechanisms are fundamentally possible and are likely to contribute to reduction of the gold over the pH range examined; although, the high pH reduction pathway by virus certainly results in maximal nanoparticle formation.

TEM examination of the nanoparticle/viral structures reveals discrete Au^0 particles associated with capsid surface of SubE (yeast), (HRE)-SubE, and wild-type, definitively confirming surface mediated gold reduction. Interestingly, several non-mineralized viral particles (Fig. 3A–D) are also present as identified by negative staining with 2% uranyl acetate; due to fast aggregative processes with other gold nanoparticle decorated viruses. Mechanistically, each virus particle rapidly reduces and generates several small Au^0 clusters per capsid which proceeds to a single cluster and then finally a large Au^0 nanoparticle from several viruses.[25] This is demonstrated in the TEM image of SubE (yeast), whereby five virus particles each contribute a Au^0 particle to the underlying engulfed capsid. Comparatively, the extent of stabilization and aggregation differentiated among the set of virus templates as determined by the average diameters of gold particles; whereby SubE (yeast), (HRE)-SubE, and wild-type yielded average gold sizes of 9.2 $\pm$ 3.9 nm, 8.33 $\pm$ 2.59 nm, and 23.8 $\pm$ 14.5 nm, respectively. The similar sizes indicate that the viral surfaces of SubE (yeast) and (HRE)-SubE are structurally and chemically similar, but different to that of wild-type due in part to variable spacings between subunits and/or surface irregularities of the wild-type virus as it is harvested from the host cowpea plant. Notably, the TEM image of Au^0/SubE from yeast reveals several encapsulated gold particles ($\sim$2%) within the viral cage. Mineralization of Au^0 nanoparticles within the empty SubE cage occurs as small gold nuclei formed by surface reduction of $AuCl_4^-$ diffuse through the viral pores. Further, the viral reduced Au^0 nanoparticles were predominantly spheroidal with a few particles displaying irregular shapes and facets. Nucleation of these shapes and facets are likely translated by the viral surface as a result of the repeating architecture of subunits in a three-dimensional organization; the conserved icosahedral symmetry of the virus with two-fold, three-fold, and five-fold symmetry; protein surface topology (*i.e.* polarity, residue charge, and surface relief); and the fluxional nature of the grafted HRE peptides (inside or outside of capsid). Ultimately, this route exploits the reductive capacity of the virus for $AuCl_4^-$, but offers little contribution to the nucleation and stabilization of particles as a result of circumventing metal ion binding due to fast reduction and aggregation.

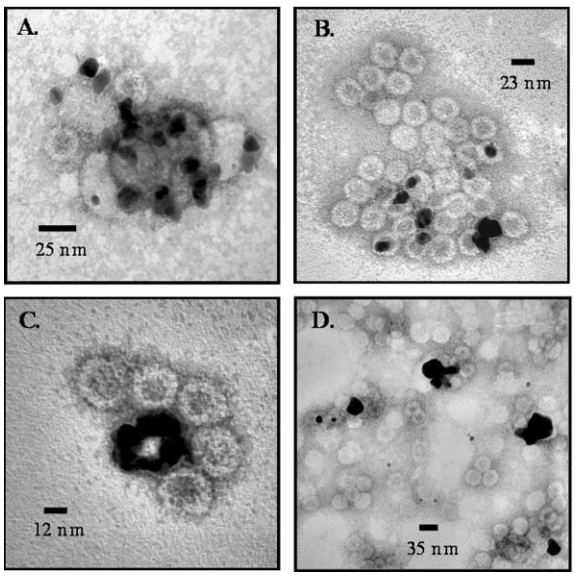

Fig. 3 TEM micrographs of gold reduction by viruses in water. (A) Au^0/(HRE)-SubE negatively stained with 2% uranyl acetate. (B) Gold reduction by SubE expressed in yeast (negatively stained). (C) SubE expressed in yeast with gold (negatively stained). (D) Gold reduced by wild-type virus (negatively stained).

Symmetry directed synthesis with $AuClP(CH_3)_3$

Alternatively, the reduction potential and solubility of $Au^IClP(CH_3)_3$ prevented reduction by the viruses, so it was examined as a viable precursor to maximize the binding efficacy of the histidine-rich virus surface. Matsui *et al.* has previously demonstrated the complete binding/saturation of $AuClP(CH_3)_3$ with an HRE engineered nanotube which displayed excellent monodispersity and surface coverage of Au^0 nanoparticles.[26] By analogy, the virus capsids contain 360 endogenous histidine residues (six histidines per subunit) that are symmetrically and structurally presented around the repeating three-fold and five-fold axes of the capsid architecture.[22] Such sites are expected to serve as excellent gold nucleation sites on the virus for the symmetry directed synthesis of gold nanoparticles in highly ordered periodic patterns. After 24 h of mixing to allow for binding/adsorption/diffusion, the precursor/virus complex was reduced by borohydride and studied by TEM. Under TEM examination (Fig. 4A), a completely decorated viral surface of gold nanoparticles was observed with gold diameters of 3.2 $\pm$ 0.9 nm for SubE (yeast), 6.21 $\pm$ 1.98 nm for (HRE)-SubE, and 4.3 $\pm$ 1.3 nm for wild-type that exhibited unique geometric patterns with interparticle spacings of $\sim$6.4 nm (metal center

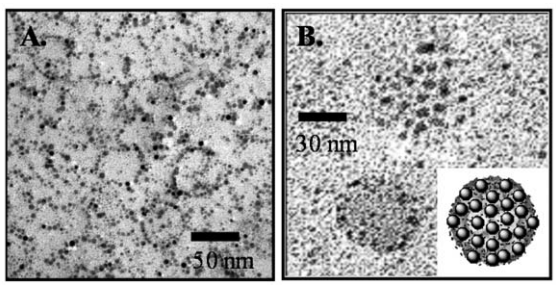

Fig. 4 TEM micrographs of virus templated synthesis of Au^0 from $AuClP(CH_3)_3$. (A) (HRE)-SubE virus with $AuClP(CH_3)_3$ and reduced by $NaBH_4$. (B) Dilute sample of (HRE)-SubE/Au^0 (inset) virus model displaying gold nanoparticle arrangement.

to metal center). These 3-D gold arrangements are more clearly observed from a dilute TEM sample (Fig. 4B) and are consistent with a nanoparticle decorated model (inset), the location specific binding of pre-formed gold nanoparticles reported by Ratna *et al.* with cowpea mosaic virus engineered with 60 and 120 cysteine residues,[27] and those studied by Braun *et al.* with silver on the surface of lumazine synthase of *Bacillus subtilus* through elaborate surface mapping and density calculations.[28] The preferential binding/nucleation of gold at these histidine-rich sites on the virus was confirmed by blocking all available histidines with diethylpyrocarbonate, a conventional protein modification agent for histidine.[29] Subsequent viral modification induced a substantial loss of binding and stabilization as noted by visible precipitation of gold. From TEM analysis, a non-periodic distribution of gold nanoparticles revealed a lack of association with the virus capsid as a result of modified histidine residues (ESI†).

We have described two viral mediated pathways to the synthesis of gold nanoparticles directed by the rich surface chemistry of the virus capsid and the selection of metal precursor, thus expanding the utility of virus particles beyond only a confined cage for synthesis. Consequently, viral reduction of gold proceeds considerably faster in comparison to reductive processes mediated by geranium leaf broth (60 min),[18] alfalfa biomass (12 h),[19] the fungus *Fusarium oxysporum* (48 h),[20] and the actinomycete *Thermomonospora* sp (120 h).[21] This new biomimetic route highlights the opportunity to exploit the reductive capacity of tyrosine for gold by introducing tyrosine residues into peptide binding domains within the viral cage or the cavities/pores of protein templates. The incorporation of tyrosine reduction sites within the viral/protein cavity or surface stabilizing peptides such as **Y**HRE or $\mathbf{Y}_4$HRE would essentially yield a complete self-contained template for the reductive synthesis of confined gold nanoparticles that could be electronically tuned by varying the ratio of tyrosine to histidine residues. While the reductive activity of the (HRE)-SubE virus for Au^{3+} precluded mineralization within the cavity, the HRE peptides lining the interior viral cage remains an encouraging template for further metal substrates not inclined to reduction by the virus. We also implemented the unique surface topology, high symmetry, and endogenous surface histidine binding/nucleation sites of the virus with a precursor ($AuClP(CH_3)_3$) that only binds to available sites on the virus as a template in the synthesis of nearly monodisperse Au^0 nanoparticles. Ultimately, the unique surface chemistry of viruses provides a means towards designing activated surfaces, integrated bioelectronic components, and hybrid materials that self-assemble in both the virus cavity and on the exterior surface.

Acknowledgements

We thank the NSF CAREER program (CHE-0304124), NSF NER program (NSF 0196540), and the Vanderbilt Institute of Nanoscale Science and Engineering for support of this work. Also, we wish to thank Mark Young and Trevor Douglas for providing virus samples and helpful discussions. RRN and MOS thank AFOSR for funding this work.

Joseph M. Slocik,[a] Rajesh R. Naik,[b] Morley O. Stone[b] and David W. Wright*[a]
[a]*Department of Chemistry, Vanderbilt University, Station B 351822, Nashville, TN, USA 37235 1822. E-mail: David.wright@vanderbilt.edu; Fax: (615) 343 1234; Tel: (615) 322 2636*
[b]*Materials and Manufacturing Directorate, Air Force Research Laboratory, Wright-Patterson Air Force Base, Dayton, OH, USA 45433 7702*

References

1 M. Allen, D. Willits, J. Mosolf, M. Young and T. Douglas, *Adv. Mater.*, 2002, **14**, 1562.
2 M. Allen, D. Willits, M. Young and T. Douglas, *Inorg. Chem.*, 2003, **42**, 6300.
3 T. Douglas, D. P. E. Dickson, S. Betteridge, J. Charnock, C. D. Garner and S. Mann, *Science*, 1995, **269**, 54.
4 T. Douglas and V. T. Stark, *Inorg. Chem.*, 2000, **39**, 1828.
5 T. Douglas, E. Strable, D. Willits, A. Aitouchen, M. Libera and M. Young, *Adv. Mater.*, 2002, **14**, 415.
6 T. Douglas and M. Young, *Nature*, 1998, **393**, 152.
7 E. Dujardin, C. Peet, G. Stubbs, J. N. Culver and S. Mann, *Nano Lett.*, 2003, **3**, 413.
8 W. Shenton, T. Douglas, M. Young, G. Stubbs and S. Mann, *Adv. Mater.*, 1999, **11**, 253.
9 M. Knez, M. Sumser, A. M. Bittner, C. Wege, H. Jeske, T. P. Martin and K. Kern, *Adv. Funct. Mater.*, 2004, **14**, 116.
10 Q. Wang, T. Lin, L. Tang, J. E. Johnson and M. G. Finn, *Angew. Chem., Int. Ed.*, 2002, **41**, 459.
11 J. M. Slocik, J. T. Moore and D. W. Wright, *Nano Lett.*, 2002, **2**, 169.
12 J. M. Slocik and D. W. Wright, *Biomacromolecules*, 2003, **4**, 1135.
13 K. Esumi, T. Hosoya, A. Suzuki and K. Torigoe, *Langmuir*, 2000, **16**, 2978.
14 Y. Zhou, W. Chen, H. Itoh, K. Naka, Q. Ni, H. Yamane and Y. Chujo, *Chem. Commun.*, 2001, 2518.
15 M. Quinn and G. Mills, *J. Phys. Chem.*, 1994, **98**, 9840.
16 O. Siiman and W. P. Hsu, *J. Chem. Soc., Faraday Trans.*, 1986, **82**, 851.
17 A. S. Ladokhin, L. Wang, A. W. Steggles and P. W. Holloway, *Biochemistry*, 1991, **30**, 10200.
18 S. S. Shankar, A. Ahmad, R. Pasricha and M. Sastry, *J. Mater. Chem.*, 2003, **13**, 1822.
19 J. L. Gardea-Torresdey, K. J. Tiemann, J. G. Parsons, G. Gamez, I. Herrera and M. Jose-Yacaman, *Microchem. J.*, 2002, **71**, 193.
20 P. Mukherjee, S. Senapati, D. Mandal, A. Ahmad, M. I. Khan, R. Kumar and M. Sastry, *ChemBioChem*, 2002, **3**, 461.
21 A. Ahmad, S. Senapati, M. I. Khan, R. Kumar and M. Sastry, *Langmuir*, 2003, **19**, 3550.
22 J. A. Speir, S. Munshi, G. Wang, T. S. Baker and J. E. Johnson, *Structure*, 1995, **3**, 63.
23 M. Sjodin, S. Styring, B. Akermark, L. Sun and L. Hammarstrom, *J. Am. Chem. Soc.*, 2000, **122**, 3932.
24 *Handbook of Chemistry and Physics*, CRC Press, Boca Raton, FL, 82nd edn., 2001.
25 M. T. Klem, D. Willits, M. Young and T. Douglas, *J. Am. Chem. Soc.*, 2003, **125**, 10806.
26 R. Djalali, Y.-F. Chen and H. Matsui, *J. Am. Chem. Soc.*, 2002, **124**, 13660.
27 A. S. Blum, C. M. Soto, C. D. Wilson, J. D. Cole, M. Kim, B. Gnade, A. Chatterji, W. F. Ochoa, T. Lin, J. E. Johnson and B. R. Ratna, *Nano Lett.*, 2004, **4**, 867.
28 N. Braun, W. Meining, U. Hars, M. Fischer, R. Ladenstein, R. Huber, A. Bacher, S. Weinkauf and L. Bachmann, *J. Mol. Biol.*, 2002, **321**, 341.
29 R. L. Lundblad, in *Techniques in Protein Modification*, CRC Press, Boca Raton, FL, 1995, pp. 105–128.